# MRCI+Q study of the low-lying electronic states of CdF including spin–orbit coupling*

Shu-Tao Zhao(赵书涛)[1,†], Bing Yan(闫冰)[2,‡], Rui Li(李瑞)[3], Shan Wu(武山)[1], and Qiu-Ling Wang(王秋玲)[1]

[1] School of Physics and Electronic Science, Fuyang Normal University, Fuyang 236037, China
[2] Jilin Provincial Key Laboratory of Applied Atomic and Molecular Spectroscopy (Jilin University), Institute of Atomic and Molecular Physics, Jilin University, Changchun 130012, China
[3] Department of Physics, College of Science, Qiqihar University, Qiqihar 161006, China

(Received 8 October 2016; revised manuscript received 20 December 2016; published online 10 January 2017)

CdF molecule, which plays an important role in a great variety of research fields, has long been subject to numerous researchers. Due to the unstable nature and heavy atom Cd containing in the CdF molecule, electronic states of the molecule have not been well studied. In this paper, high accurate *ab initio* calculations on the CdF molecule have been performed at the multi-reference configuration interaction level including Davidson correction (MRCI+Q). Adiabatic potential energy curves (PECs) of the 14 low-lying Λ–S states correlating with the two lowest dissociation limits $Cd(^1S_g)+F(^2P_u)$ and $Cd(^3P_u)+F(^2P_u)$ have been constructed. For the bound Λ–S and Ω states, the dominant electronic configurations and spectroscopic constants are obtained, and the calculated spectroscopic constants of bound states are consistent with previous experimental results. The dipole moments (DMs) of $^2\Sigma^+$ and $^2\Pi$ are determined, and the spin–orbit (SO) matrix elements between each pair of $X^2\Sigma^+$, $2^2\Sigma^+$, $1^2\Pi$, and $2^2\Pi$ are obtained. The results indicate that the sudden changes of DMs and SO matrix elements arise from the variation of the electronic configurations around the avoided crossing region. Moreover, the Franck–Condon factors (*FCFs*), the transition dipole moments (TDMs), and radiative lifetimes of low-lying states-the ground state $X^2\Sigma^+$ are determined. Finally, the transitional properties of $2^2\Pi$–$X^2\Sigma^+$ and $2^2\Sigma^+$–$X^2\Sigma^+$ are studied. Based on our computed spectroscopic information of CdF, the feasibility and challenge for laser cooling of CdF molecule are discussed.

**Keywords:** CdF, spin–orbit coupling effect, potential energy curves, spectroscopic constant

**PACS:** 31.50.Df, 31.15.aj, 31.15.ag **DOI:** 10.1088/1674-1056/26/2/023105

## 1. Introduction

The halides of group IIB (Zn and Cd) have attracted much attention due to their significant roles in a number of research fields.[1] As the candidates generating chemical laser, the excited states of the halides of Cd have been extensively investigated.[2] In addition, zinc is a significant element for biological systems and synthetic organic chemistry; and also is an important kind of transition metals in the human body, which is related to nerve disease such as Alzheimer's disease.[3,4] Another motivation is to seek the potential candidate molecules for laser cooling. Because of the similar valence electronic structure with the first experimentally laser-cooled molecule SrF,[5] the cadmium halides have attracted a growing theoretical and experimental interest. The information on electronic structures and transition properties for the halides of group IIB elements is helpful to reveal the bonding nature between group IIB metal and halogen atoms, therefore much theoretical and experimental effort has been made in previous works.[6–8]

The transitional properties of halides of Zn and Cd were mainly focused on $2^2\Sigma^+$–$X^2\Sigma^+$ and $2^2\Pi$–$X^2\Sigma^+$ band systems. Early in 1939, the ultraviolet absorption spectra of ZnF were detected by Rochester and Olsson, and were assigned to a transition from $^2\Pi$ excited state.[9] Later, a number of experimental works on the electronic states of halides of Zn were carried out. Moravec *et al.*[10] observed anion photoelectron spectroscopy of ZnF and evaluated the spectroscopic parameters of the ground state $X^2\Sigma^+$. Subsequently, the pure rotational spectrum of the $X^2\Sigma^+$ state was detected by Flory *et al.*,[11] and the excitation energy of $A^2\Pi$ state was measured. In contrast to those on ZnF, the experimental spectroscopy investigations on CdF are less extensively. Two emission bands in CdF, yellow–green and orange bands, were firstly detected by Asundi *et al.*[12] Later, Fowler recorded the absorption spectrum in the wavelength range of 2716.2 Å–2923.5 Å,[13] and this spectrum band was tentatively assigned to $2^2\Sigma^+$–$X^2\Sigma^+$ transition by Huber *et al.*[14]

On the other hand, a series of theoretical investigations

*Project supported by the National Natural Science Foundation of China (Grant Nos. 11604052, 11404180, and 11574114 ), the Natural Science Foundation of Heilongjiang Province, China (Grant No. A2015010), the Natural Science Foundation of Anhui Province, China (Grant No. 1608085MA10), the International Science & Technology Cooperation Program of Anhui Province, China (Grant No. 1403062027), the University Nursing Program for Young Scholars with Creative Talents in Heilongjiang Province, China (Grant No. 2015095), and the Natural Science Foundation of Jilin Province, China (Grant No. 20150101003JC).

†Corresponding author. E-mail: zhaoshutao2002@163.com
‡E-mail: yanbing@jlu.edu.cn

© 2017 Chinese Physical Society and IOP Publishing Ltd 

were made on the electronic structures of low-lying states of ZnF over the past several decades. Bowmaker *et al.* carried out HF (Hartree–Fock)/CI (Configuration Interaction) pseudopotential calculations on the electronic structure of the ground state $X^2\Sigma^+$, and reported the dissociation energy and equilibrium bond length.[15] Harrison *et al.* obtained vibrational constants of the ground state by high-level RCCSD(T) approach.[16] Hayashi systematically investigated the electronic states correlating to the two lowest dissociation limits of ZnF with MRCI calculations, and determined the electronic structures and DMs of these electronic states.[17] While the CdF, as the isovalent molecular system of ZnF, is less extensively investigated. Kaupp *et al.* computed the geometry structure of CdF utilizing HF method and $MP_2$ (Møller–Plesset theory, 2nd order) method.[18] Liao *et al.* calculated the electronic structure of the $X^2\Sigma^+$ state of CdF, employing the relativistic density-functional method, and they gave the vibrational frequency and bond length of the $X^2\Sigma^+$ state.[19] The previous theoretical investigations on the CdF were mainly focused on the ground state $X^2\Sigma^+$. Hence, the interaction of the excited states of the molecule is still unclear.

As discussed above, the electronic structures of low-lying electronic states of ZnF have been extensively studied in previous works. However, the information on the excited states of CdF is still limited, especially in the theoretical investigations. In previous ab initio calculations on ZnF, the spin–orbit coupling (SOC) effect and core-valence (CV) electrons correlations were neglected. However, the SOC effect and CV correlations play key roles in the electronic states of molecules.[20–25] Therefore, it is essential to undertake configuration interaction study on the electronic states and transition properties of the CdF with inclusion of SOC and CV correlations.

In this paper, high-level configuration interaction computations were carried out on the electronic structure and transition properties of the low-lying electronic states of CdF. The CV correlation effects of the $4d^{10}$ electrons for Cd atom were also taken into consideration in the calculations. The PECs of the 14 Λ–S states correlating with the two lowest dissociation asymptotes of CdF as well as 30 $\Omega$ states generated from these Λ–S states were determined. Based on the computed PECs, the various spectroscopic parameters of the bound Λ–S and $\Omega$ states, most of which have not been presented in the literature so far, were evaluated. The transitional properties of $2^2\Pi$–$X^2\Sigma^+$ as well as $2^2\Sigma^+$–$X^2\Sigma^+$ were illuminated and the *R*-dependent Λ–S compositions of the $\Omega = (3)1/2$ and $(4)1/2$ states were also discussed. Finally, we deduced radiative lifetimes of several low-lying vibrational levels of CdF molecule from the calculated PECs and transition moments. We expect further experimental study on the electronic structures and transition properties motivated by present computational work.

## 2. Calculation method

In this paper, the electronic structures of CdF were computed with the MOLPRO 2010 software package.[26] The point group of CdF is $C_{\infty v}$ symmetry. Owing to the limit of the software package, the calculations of electronic structures were performed in the $C_{2v}$ symmetry. The relations of the irreducible representations for $C_{2v}$ and $C_{\infty v}$ are $\Sigma^+ = A_1$, $\Pi = B_1 + B_2$, $\Delta = A_1 + A_2$ and $\Sigma^- = A_2$. By solving one-dimensional Schrödinger equations using the LEVEL program,[27] the spectroscopic constants of CdF were determined. The single-point energies of electronic states of CdF were computed to construct the PECs. For the heavy atom Cd, the usage of effective potentials should be required. Therefore, the contracted Gaussian-type basis set aug-cc-pwCVQZ-PP (ECP28MDF) of Cd[28] was chosen. For the F atom the contracted Gaussian-type basis set aug-cc-pVQZ[29] was used. A series of calculations were carried out as followed: Firstly, the HF method was used to obtain the wavefunction of the ground state; secondly, the multi-configuration wavefunction was derived using the state-averaged complete active space self-consistent field (SA-CASSCF) approach.[30] Finally, the icMRCI + Q method[31,32] was used to consider the dynamical electron correlation and reduce the size-consistency error. In the CASSCF calculation, $3a_1$, $2b_1$, and $2b_2$ molecular orbitals (MOs) are chosen as the active space, which are correlated with the 5s5p(Cd) and 2p(F) atomic orbitals. The outermost $5s^2$ electrons of the Cd atom and $2p^5$ of the F atom were put into the active space. The $4d^{10}$ electrons of Cd atom and the $2s^2$ of F atom were correlated, which were taken into account for the CV correlation effect. That is, a total of 19 electrons in the CdF were correlated in present calculations.

The SOC effect was taken into consideration by state-interacting approach employing the Breit–Pauli Hamiltonian.[33] The SO matrix was determined in the SOC calculations. The off-diagonal SO matrix elements were obtained from the CASSCF wavefunctions and the diagonal SO matrix elements were replaced by the MRCI + Q energies. After taking account of SOC effects, 30 $\Omega$ states were generated from the 14 Λ–S states of CdF. The PECs of the 14 Λ–S and 30 $\Omega$ states were mapped with the aid of the avoided crossing rule.

Based on the computed PECs of the Λ–S states, we evaluated Einstein coefficients and *FCFs* of the $2^2\Pi$–$X^2\Sigma^+$ and $2^2\Sigma^+$–$X^2\Sigma^+$ transitions. The TDMs and DMs were computed from the wavefunctions and energies of icMRCI level. Based

on the computed TDMs, *FCFs*, and energy separation between different vibrational levels, the radiative lifetimes of the low-lying vibrational levels were computed.

## 3. Results and discussion

### 3.1. PECs of the 14 Λ–S states

The 14 Λ–S electronic states correlating with the two lowest dissociation asymptotes $Cd(^1S_g)+F(^2P_u)$ and $Cd(^3P_u)+F(^2P_u)$ were computed with the icMRCI+Q method. The ground state $X^2\Sigma^+$ and the $1^2\Pi$ state correlate with the lowest asymptote $Cd(^1S_g)+F(^2P_u)$. Other twelve molecular states (two $^{2,4}\Sigma^+$, one $^{2,4}\Sigma^-$, two $^{2,4}\Pi$, and one $^{2,4}\Delta$) correlate with the second asymptote $Cd(^3P_u)+F(^2P_u)$. The energy difference of the second and the first dissociation limit is 30147 $cm^{-1}$, which fits well with the experimental value[34] of 31246 $cm^{-1}$. The PECs of the doublet and quartet states of CdF at the icMRCI+Q level were plotted in Figs. 1 and 2, respectively. The computation step length of PECs was set at 0.05 Å for $R = 1.3$–3.8, 0.1 Å for $R = 3.8$–4.5, 0.5 Å for $R = 4.5$–5.0, and 1.0 Å for $R = 5.0$–6.0. The spectroscopic parameters ($R_e$, $\omega_e$, $\omega_e x_e$, $T_e$, $B_e$, $D_e$) were determined and given in Table 1.

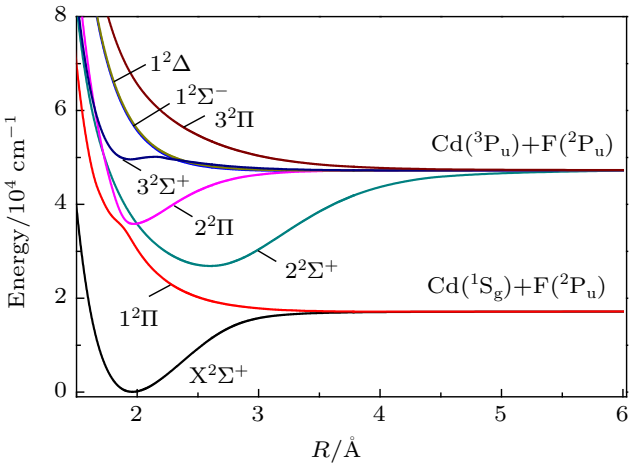



**Fig. 1.** (color online) MRCI+Q potential energy curves of the doublet states of CdF molecule.

**Table 1.** Spectroscopic constants of the Λ–S states of CdF.

| State | $T_e$/$cm^{-1}$ | $\omega_e$/$cm^{-1}$ | $\omega_e x_e$/$cm^{-1}$ | $B_e$/$cm^{-1}$ | $R_e$/Å | $D_e$/eV | Configuration at $R_e$/% | |
|---|---|---|---|---|---|---|---|---|
| $X^2\Sigma^+$ | 0 | 549.2126 | 2.5792 | 0.2704 | 1.9594 | 2.1281 | $6\sigma^2 7\sigma^1 8\sigma^0 3\pi^4 4\pi^0$ | (72.1) |
| | | | | | | | $6\sigma^1 7\sigma^2 8\sigma^0 3\pi^4 4\pi^0$ | (9.3) |
| | | | | | | | $6\sigma^2 7\sigma^0 8\sigma^1 3\pi^4 4\pi^0$ | (5.0) |
| Expt. | | 535[a] | | | | | | |
| Calc. | | 508[b] | | | 2.016[b] | | | |
| $2^2\Sigma^+$ | 26854.0838 | 315.4002 | 0.5845 | 0.1537 | 2.5985 | 2.5216 | $6\sigma^1 7\sigma^2 8\sigma^0 3\pi^4 4\pi^0$ | (73.4) |
| | | | | | | | $6\sigma^2 7\sigma^1 8\sigma^0 3\pi^3 4\pi^1$ | (8.8) |
| | | | | | | | $6\sigma^2 7\sigma^0 8\sigma^1 3\pi^4 4\pi^0$ | (4.5) |
| Expt. | 34200[a] | 535[a] | | | | | | |
| $2^2\Pi$ | 35740.9601 | 657.2600 | 8.9027 | 0.2684 | 1.9657 | 1.4303 | $6\sigma^2 7\sigma^0 8\sigma^0 3\pi^4 4\pi^1$ | (61) |
| | | | | | | | $6\sigma^1 7\sigma^1 8\sigma^0 3\pi^4 4\pi^1$ | (27.8) |
| $3^2\Sigma^+$ | 49554.3551 | | | | 1.9407 | 0.0713 | $6\sigma^2 7\sigma^0 8\sigma^1 3\pi^4 4\pi^0$ | (44) |
| | | | | | | | $6\sigma^2 7\sigma^1 8\sigma^0 3\pi^3 4\pi^1$ | (19.8) |
| | | | | | | | $6\sigma^1 7\sigma^1 8\sigma^1 3\pi^4 4\pi^0$ | (12.8) |
| $1^2\Delta$ | 47112.9257 | 33.7057 | 1.8149 | 0.0877 | 3.4423 | 0.0185 | $6\sigma^2 7\sigma^1 8\sigma^0 3\pi^3 4\pi^1$ | (97.7) |
| $1^2\Sigma^-$ | 47218.2814 | 23.6328 | 2.0200 | 0.0765 | 3.6904 | 0.0080 | $6\sigma^2 7\sigma^1 8\sigma^0 3\pi^3 4\pi^1$ | (97.8) |
| $1^4\Sigma^+$ | 46778.5340 | 60.8909 | 2.0393 | 0.1159 | 2.9945 | 0.0585 | $6\sigma^2 7\sigma^1 8\sigma^0 3\pi^3 4\pi^1$ | (98.1) |
| $1^4\Delta$ | 47055.5624 | 44.6820 | 2.1825 | 0.1015 | 3.2044 | 0.0278 | $6\sigma^2 7\sigma^1 8\sigma^0 3\pi^3 4\pi^1$ | (98.3) |
| $1^4\Sigma^-$ | 47196.2115 | 29.2261 | 2.2180 | 0.0867 | 3.4664 | 0.0115 | $6\sigma^2 7\sigma^1 8\sigma^0 3\pi^3 4\pi^1$ | (98.1) |

[a] Ref. [14], [b] Ref. [19].

Because of the effective core potential used in this paper, the inner $1s^2 2s^2 2p^6 3s^2 3p^6 3d^{10}$ electrons of Cd atom kept in the $n = 1$–3 shells are represented by means of a pseudopotential. Thus, the $n = 1$–3 shells were not included in the MOs. The 1–5$\sigma$, 1$\delta$, and 1–2$\pi$ MOs, corresponding to the Cd 4s4p4d and F 1s2s orbitals, are kept doubly occupied in CASSCF calculations. The constructions of 6–8$\sigma$ and 3–4$\pi$ orbitals are as follows: the bonding 6$\sigma$ and antibonding 7$\sigma$ orbital correspond to a combination of the $2p_z$ of F and the 5s of Cd. The $2p_z$ of F mainly contributes to the 6$\sigma$ orbital, while the 5s of Cd mainly contributes to the 7$\sigma$. The 8$\sigma$ orbital is more diffuse and is mainly arising from the $5p_z$ of Cd. The 3$\pi$ and 4$\pi$ orbitals correspond to the F $2p_x 2p_y$ and Cd $5p_x 5p_y$ atomic orbitals, respectively.

As shown in Fig. 1 and Fig. 2, from these calculated PECs, there are nine bound states ($X^2\Sigma^+$, $2^2\Sigma^+$, $2^2\Pi$, $3^2\Sigma^+$, $1^2\Delta$, $1^2\Sigma^-$, $1^4\Sigma^+$, $1^4\Delta$, $1^4\Sigma^-$) and five repulsive states ($1^2\Pi$, $3^2\Pi$, $2^4\Sigma^+$, $1^4\Pi$, $2^4\Pi$). The ground state $X^2\Sigma^+$ of CdF correlating with the lowest asymptote has an equilibrium geometry around $R = 1.95$ Å. The strong interaction of $X^2\Sigma^+$ with $2^2\Sigma^+$ is presented in the region near $R = 2.60$ Å, which leads to a deep minimum for the $2^2\Sigma^+$ state at $R = 2.60$ Å, and an-

other $3^2\Sigma^+$ state correlating with the second asymptote shows a shallow minimum at $R = 1.95$ Å. The $1^2\Pi$ and $2^2\Pi$ states correlating with different asymptotes form an avoided crossing point at the internuclear distance near $R = 1.90$ Å. Such avoided crossing phenomenon will be analyzed in the following discussion. The $1^2\Pi$ state is unbound but has a potential barrier at the avoided crossing point. The minimum for the $2^2\Pi$ state lies at $R = 1.95$ Å, which is caused by the avoided crossing phenomenon between $2^2\Pi$ and $1^2\Pi$ states. As shown in Figs. 1 and 2, $3^2\Pi$, $2^4\Sigma^+$, $1^4\Pi$, $2^4\Pi$ and $1^2\Delta$, $1^2\Sigma^-$, $1^4\Sigma^+$, $1^4\Delta$, $1^4\Sigma^-$ are repulsive and bound, respectively, which are associated with the second asymptote.

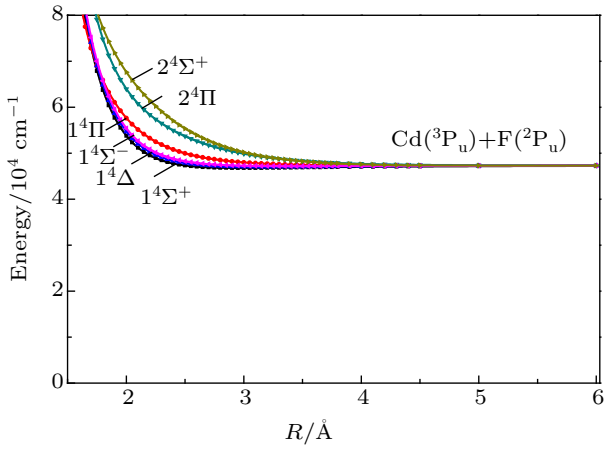



**Fig. 2.** (color online) MRCI+Q potential energy curves of the quartet states of CdF molecule.

Previously, only the vibrational constant $\omega_e$ of the ground state $X^2\Sigma^+$ and spectroscopic constants ($T_e$ and $\omega_e$) of the excited state $2^2\Sigma^+$ were experimentally reported. As listed in Table 1, the $X^2\Sigma^+$ state is mainly from the electronic configuration $6\sigma^2 7\sigma^1 8\sigma^0 3\pi^4 4\pi^0$ (72%) with a small amount of mixtures from $6\sigma \rightarrow 7\sigma$ and $7\sigma \rightarrow 8\sigma$ transitions. Our computed vibrational constant $\omega_e$ of the $X^2\Sigma^+$ at the icMRCI+Q level differs from the experimental result[14,35] by only 14.2126 cm$^{-1}$, and are 41.2126 cm$^{-1}$ larger than previous theoretical value.[19] The equilibrium distance of $X^2\Sigma^+$ is calculated to be 1.9594 Å, which is well consistent with existing theoretical result of 2.016 Å.[19] The $2^2\Sigma^+$ state mainly arises from the electronic configuration $6\sigma^1 7\sigma^2 8\sigma^0 3\pi^4 4\pi^0$ (73.4%), which corresponds to a single-electron transition of $6\sigma \rightarrow 7\sigma$.

For the $2^2\Sigma^+$–$X^2\Sigma^+$ transition, the experimental values of $T_e$ and $\omega_e$ are uncertain as summarized by Huber and Herzberg.[14] Our results of $T_e$ and $\omega_e$ of $2^2\Sigma^+$ are 26854 cm$^{-1}$ and 315 cm$^{-1}$, respectively, which are obviously smaller than those from the corresponding experimental results (34200 cm$^{-1}$ and 535 cm$^{-1}$).[14] As illustrated in Table 2, the energy separations of the eight lowest dissociation limits are reasonably consistent with experimental atomic energy level,[34] hence, we expect presently computed spectroscopic constants of $2^2\Sigma^+$ are more reliable. In contrast, the present $T_e$ and $B_e$ of $2^2\Pi$ state are 35740 cm$^{-1}$ and 657 cm$^{-1}$, which are close to the experimental results (34200 cm$^{-1}$ and 535 cm$^{-1}$) of the $2^2\Sigma^+$. Since $2^2\Pi$–$X^2\Sigma^+$ transition has large transition dipole moment in the Franck–Condon region (see Fig. 9), the $2^2\Pi$–$X^2\Sigma^+$ transition can also be easily observed in experiment. Therefore, the $2^2\Sigma^+$ state tentatively identified in previous experimental work should be the $2^2\Pi$ state according to the present computational results. For the other electronic states, the electronic structures have not been reported in the literature. Our calculated results of the spectroscopic constants can provide theoretical help for the future experimental studies.

**Table 2.** Dissociation relationgship of the low-lying $\Omega$ states of CdF.

| Atomic state (Cd + F) | $\Omega$ state | Energy/cm$^{-1}$ | |
|---|---|---|---|
| | | This work | Expt.[a] |
| $^1S_0+^2P_{3/2}$ | 3/2, 1/2 | 0 | 0 |
| $^1S_0+^2P_{1/2}$ | 1/2 | 394 | 404 |
| $^3P_0+^2P_{3/2}$ | 3/2, 1/2 | 29105 | 30114 |
| $^3P_0+^2P_{1/2}$ | 1/2 | 29500 | 30517 |
| $^3P_1+^2P_{3/2}$ | 5/2, 3/2, 3/2, 1/2, 1/2, 1/2, | 29623 | 30656 |
| $^3P_1+^2P_{1/2}$ | 3/2, 1/2, 1/2 | 30014 | 31060 |
| $^3P_2+^2P_{3/2}$ | 7/2, 5/2, 5/2, 3/2, 3/2, 3/2, 1/2, 1/2, 1/2, 1/2 | 30624 | 31827 |
| $^3P_2+^2P_{1/2}$ | 5/2, 3/2, 3/2, 1/2, 1/2 | 31025 | 32231 |

[a]Ref. [34].

The leading electronic configurations and their weights of selected bound states are listed in Table 1. At large bond length, the leading electronic configuration for the $X^2\Sigma^+$ is $6\sigma^1 7\sigma^2 8\sigma^0 3\pi^4 4\pi^0$, which reveals the covalent situation of the $X^2\Sigma^+$ of CdF. In the internuclear distance between 1.3 Å and 2.4 Å, the leading configuration of the $X^2\Sigma^+$ state is $6\sigma^2 7\sigma^1 8\sigma^0 3\pi^4 4\pi^0$, correlating to a single electron transfer from Cd to F. While the leading configuration of $2^2\Sigma^+$ state changes into $6\sigma^1 7\sigma^2 8\sigma^0 3\pi^4 4\pi^0$ induced by the avoided crossing occurring with $X^2\Sigma^+$ around $R = 2.6$ Å. At larger distance $R = 3.0$ Å, the main configuration of the $2^2\Sigma^+$ state is $6\sigma^2 7\sigma^1 8\sigma^0 3\pi^4 4\pi^0$ with a coefficient of 0.52, which is the same with those of ground state $X^2\Sigma^+$ in short internuclear distance, indicating ionic structure of $2^2\Sigma^+$ state at large internuclear distance. According to the analysis of its electronic configuration, the $3^2\Sigma^+$ state exhibits ionic characters at its equilibrium geometry, indicating the single electron transfer is favored in excited state.

At internuclear distances larger than $R = 1.95$ Å, the leading configuration of the $1^2\Pi$ state is $6\sigma^2 7\sigma^2 8\sigma^0 3\pi^3 4\pi^0$, while the $2^2\Pi$ state is characterized by $6\sigma^2 7\sigma^0 8\sigma^0 3\pi^4 4\pi^1$. These leading configurations are associated with Cd($4d^{10}5s^2$)+F($2s^2 2p^5$) for $1^2\Pi$ state and

$Cd^+(4d^{10}5p^1)+F^-(2s^22p^6)$ for the $2^2\Pi$ state. At internuclear distances shorter than 1.85 Å, the dominant configurations of $1^2\Pi$ and $2^2\Pi$ are $6\sigma^27\sigma^08\sigma^03\pi^44\pi^1$ and $6\sigma^27\sigma^28\sigma^03\pi^34\pi^0$, respectively. The dominant configurations are interchanged at bond length shorter than 1.85 Å, owing to the avoided crossing phenomenon between these two $^2\Pi$ states near 1.9 Å.

For these $^2\Sigma^+$ and $^2\Pi$ states, the dipole moment curves were also calculated at the icMRCI level and mapped in Figs. 3 and 4, respectively. With the help of the dipole moment curves, we discuss the interactions and polarity of the states. As shown in Fig. 3, the charge separation of the $X^2\Sigma^+$ state in the bonding range of $R = 1.95$ Å is close to $0.87e$, illuminating the $Cd^{\delta+}F^{\delta-}$ polarity. Our calculated dipole moment of the $X^2\Sigma^+$ state (0.87 a.u., the unit a.u. is short for atomic unit) is consistent with that of isovalent molecule ZnF (0.77 a.u.).[17] In the distance near 2.3 Å, the dipole moment reaches the largest magnitude and then the absolute value decreases to zero as distance $R$ larger than 3.3 Å, which is associated with the covalent dissociation limit. For distance longer than 5.0 Å, the dipole moment of $2^2\Sigma^+$ tends to be zero, corresponding to the covalent structure. For distance $R = 3.0$ Å–5.0 Å, the $2^2\Sigma^+$ exhibits an ionic $Cd^{\delta+}F^{\delta-}$ polarity with a largest value of the dipole moment near $R = 3.2$ Å. The interaction between $2^2\Sigma^+$ state and $X^2\Sigma^+$ leads to the exchange of their ionic characters in the avoided crossing region. The polarity change of the $X^2\Sigma^+$ and $2^2\Sigma^+$ states is arising from the charge transfer in the electronic configuration $6\sigma^27\sigma^18\sigma^03\pi^44\pi^0$. For distance longer than 3.3 Å, the dipole moment of the $3^2\Sigma^+$ tends to be zero, correlating to the covalent structure. In the equilibrium distance of this state, the dipole moment is positive, indicating an ionic $Cd^{\delta+}F^{\delta-}$ polarity. As depicted in Fig. 4, the abrupt gradient change for the dipole moment of the $1^2\Pi$ and $2^2\Pi$ locates at about $R = 1.90$ Å, owing to the drastic change of the wavefunctions around the avoided crossing region mentioned above. The weights $c^2$ of the dominated electronic configurations (con-A, con-B) of these two electronic states as a function of the interatomic distance were presented in Fig. 5. As shown in Fig. 5, the con-B plays key role in the $1^2\Pi$ state at small distance, but reduces rapidly around the avoided crossing region. In contrast, the con-A is almost equal to zero at short distance, but increases rapidly near the avoided crossing region. For these two $^2\Pi$ states, the weights $c^2$ of each main configuration present abrupt changes in the avoided crossing region. The dominant electronic configurations are exchanged around the avoided crossing, which means the interchange of the wavefunctions for the two states, hence leading to the sudden changes of the dipole moment. At distances longer than 1.9 Å, the dipole moment of the $2^2\Pi$ state is positive with a largest value near $R = 2.0$ Å, corresponding to the ionic structure of $Cd^{\delta+}F^{\delta-}$ type. The $Cd^{\delta+}F^{\delta-}$ polarity of the $2^2\Pi$ state originates from the singlet electron transfer from Cd to F appearing in the configuration $6\sigma^27\sigma^08\sigma^03\pi^44\pi^1$. For distance longer than 5 Å, the $3^2\Pi$ state exhibits a covalent structure, corresponding to the quasi-zero result of the dipole moment. In the region $R = 1.9$ Å–5.0 Å, the dipole of the $3^2\Pi$ state is negative, corresponding to the ionic structure of $Cd^{\delta-}F^{\delta+}$ type.

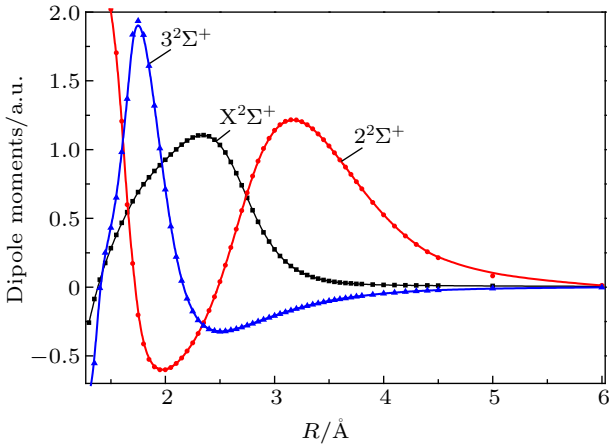



**Fig. 3.** (color online) Evolution of dipole moments of $^2\Sigma^+$ states of CdF at the MRCI level.

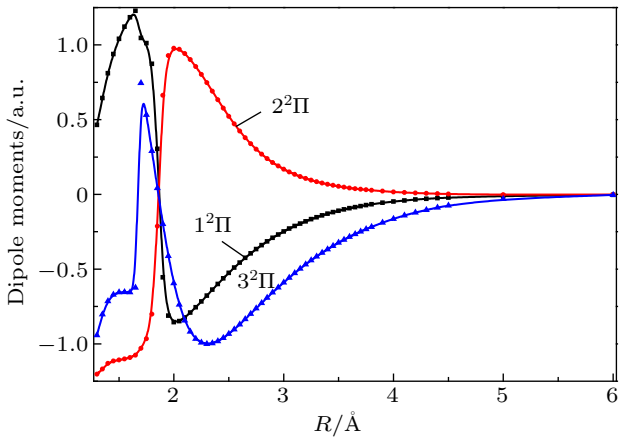



**Fig. 4.** (color online) Evolution of dipole moments of $^2\Pi$ states of CdF at the MRCI level.

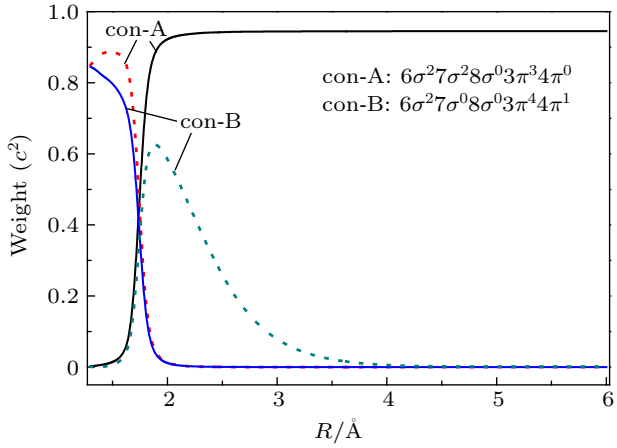



**Fig. 5.** (color online) The weights $c^2$ of the mainly electronic configurations of the $1^2\Pi$ state (solid lines) and the $2^2\Pi$ state (dot lines) as a function of the internuclear distance.

### 3.2. PECs of the 30 $\Omega$ states

As mentioned above, the PECs of Λ–S states were obtained by solving the Hamiltonian with the Born–Oppenheimer approximation, while the spin-dependent part was neglected. For the heavy metal fluoride CdF, the SOC effect on multiplet state are obvious. The SOC effect make the strong interactions for Λ–S states of the heavy metal fluoride CdF, especially the electronic states involving the PECs' avoided crossing and intersection region. To quantitatively evaluate the interactions, the value of SO matrix elements were evaluated, and the evolution of SO matrix elements between each pair of $X^2\Sigma^+$, $2^2\Sigma^+$, $1^2\Pi$, and $2^2\Pi$ were plotted in Fig. 6. As shown in Fig. 6, the significant change could be observed around the region $R = 1.9$ Å and 2.3 Å, which could arise from the abrupt change of electronic configurations in the avoided crossing region mentioned above.

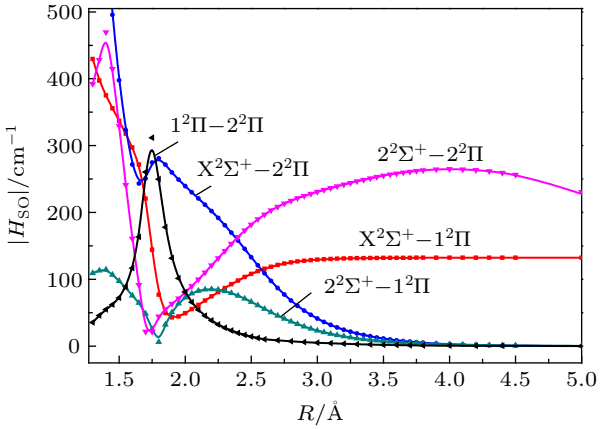



**Fig. 6.** (color online) The absolute $R$-dependent SO elements of the $X^2.\Sigma^+$, $2^2.\Sigma^+$, $1^2\Pi$, and $2^2\Pi$.

After taking into account of the spin–orbit coupling effects, a given multiplet Λ–S state splits into several $\Omega$ states. The same $\Omega$ components of the Λ–S states form avoided crossings. Due to the spin–orbit coupling effect, the dissociation limits $Cd(^1S_g)+F(^2P_u)$ and $Cd(^3P_u)+F(^2P_u)$ split into $Cd(^1S_0)+F(^2P_{3/2})$, $Cd(^1S_0)+F(^2P_{1/2})$, $Cd(^3P_0)+F(^2P_{3/2})$, $Cd(^3P_0)+F(^2P_{1/2})$, $Cd(^3P_1)+F(^2P_{3/2})$, $Cd(^3P_1)+F(^2P_{1/2})$, $Cd(^3P_2)+F(^2P_{3/2})$, and $Cd(^3P_2)+F(^2P_{1/2})$. The energy separation of higher dissociation limits with respect to the lowest dissociation limit $Cd(^1S_0)+F(^2P_{3/2})$ are calculated to be 394, 29105, 29500, 29623, 30014, 30624, and 31025 $cm^{-1}$, respectively, differing from the corresponding experimental results[34] by only 10 $cm^{-1}$(2%), 1009 $cm^{-1}$(3%), 1017 $cm^{-1}$(3%), 1033 $cm^{-1}$(3%), 1046 $cm^{-1}$(3%), 1203 $cm^{-1}$(4%), 1206 $cm^{-1}$(4%). There are 30 states with $\Omega = 1/2, 3/2, 5/2, 7/2$, corresponding to the eight low-lying dissociation limits. The relationship of computational $\Omega$ states with their dissociation limits is listed in Table 2.

The PECs of the $\Omega = 1/2$ and $\Omega = 3/2, 5/2, 7/2$ states were plotted in Fig. 7 and 8, respectively. The spectroscopic constants of the bound $\Omega$ states were evaluated and listed in Table 3. The ground state $X^2\Sigma^+_{1/2}$ is completely consisted of the $X^2\Sigma^+$ state, so their spectroscopic constants are almost the same as that of $X^2\Sigma^+$ state. For most of the other states, their spectroscopic parameters would be revised due to the avoided crossing phenomenon and the change of the PECs' shape, as compared to those of the pure Λ–S states. The SOC splitting of the $2^2\Pi$ leads to the $\Omega$ state $2^2\Pi_{1/2}((3)1/2)$ and $2^2\Pi_{3/2}((2)3/2)$. It can be seen from Fig. 7, there is an avoided crossing around $R = 2$ Å between the $2^2\Pi_{1/2}$ and $2^2\Sigma^+_{1/2}(4(1/2))$ states as a result of their common $\Omega = 1/2$ component. Owing to the avoided crossing phenomenon, the $2^2\Sigma^+_{1/2}$ state potential well shifts higher by 9385 $cm^{-1}$ and the bond length shortens by 0.59 Å than the $2^2\Sigma^+$ state, respectively. In order to further illuminate the influence of SOC effect on the PECs, the change of Λ–S compositions of the $\Omega = (3)1/2$ and $(4)1/2$ states are shown in Table 4 in the range of 1.8 Å–2.2 Å. For the two $\Omega$ states, the dominant Λ–S compositions exchange between the $2^2\Sigma^+$ and $2^2\Pi$ states at the avoided crossing region near $R = 2.05$ Å.

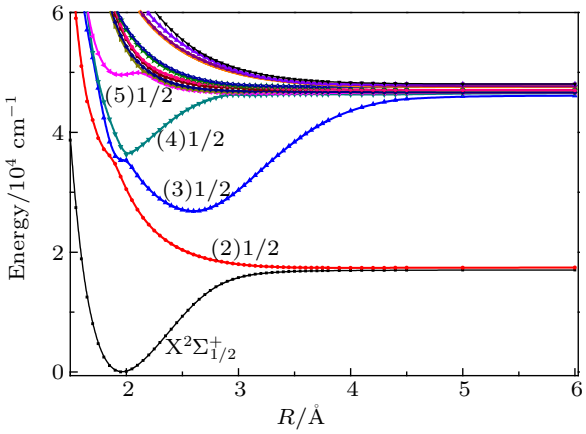



**Fig. 7.** (color online) The potential energy curves of the $\Omega = 1/2$ states of the CdF.

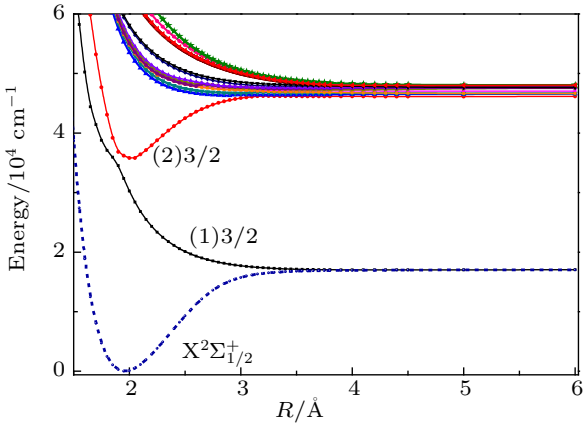



**Fig. 8.** (color online) The potential energy curves of the $\Omega = 3/2, 5/2, 7/2$ states of the CdF.

**Table 3.** Spectroscopic constants of the bound $\Omega$ states of the CdF.

| State | $T_e$/cm$^{-1}$ | $\omega_e$/cm$^{-1}$ | $\omega_e x_e$/cm$^{-1}$ | $B_e$/cm$^{-1}$ | $R_e$/Å | $D_e$/eV | Dominant Λ–S composition at $R_e$/% |
|---|---|---|---|---|---|---|---|
| (1)1/2 | 0 | 549.2430 | 2.5796 | 0.2704 | 1.9594 | 2.1127 | $X^2\Sigma^+$ (99.9) |
| (3)1/2 | 26846.4586 | 315.4279 | 0.5919 | 0.1537 | 2.5988 | 2.3925 | $2^2\Pi_{1/2}$ (99.6), $2^2\Sigma^+_{1/2}$ (0.21) |
| (2)3/2 | 35730.2460 | 625.3230 | 8.0225 | 0.2540 | 2.0241 | 1.2865 | $2^2\Pi_{3/2}$ (99.92), $1^2\Pi_{3/2}$ (0.06), |
| (4)1/2 | 36239.7449 | 841.4501 | 23.3004 | 0.2583 | 2.0083 | 1.2776 | $2^2\Sigma^+_{1/2}$ (99.74), $2^2\Pi_{1/2}$ (0.2) |
| (5)1/2 | 49568.2442 | | | | 1.9449 | 0.0425 | $3^2\Sigma^+_{1/2}$ (99.90), $2^2\Pi_{1/2}$ (0.06) |

**Table 4.** Composition of $\Omega = (3)1/2$, $(4)1/2$ states of CdF at some selected bond distances.

| State | $r$/Å | $2^2\Sigma^+$ | $2^2\Pi$ |
|---|---|---|---|
| (3)1/2 | 1.80 | 0.06 | 99.62 |
| | 1.85 | 0.05 | 99.26 |
| | 1.90 | 0.07 | 98.70 |
| | 1.95 | 0.21 | 99.60 |
| | 2.0 | 7.76 | 92.18 |
| | 2.05 | 99.34 | 0.06 |
| | 2.10 | 99.79 | 0.14 |
| | 2.15 | 99.86 | 0.08 |
| | 2.2 | 99.88 | 0.06 |
| (4)1/2 | 1.80 | 99.92 | 0.06 |
| | 1.85 | 99.93 | 0.04 |
| | 1.90 | 99.9 | 0.06 |
| | 1.95 | 99.74 | 0.2 |
| | 2.0 | 92.18 | 7.74 |
| | 2.05 | 0.59 | 99.34 |
| | 2.10 | 0.15 | 99.78 |
| | 2.15 | 0.08 | 99.84 |
| | 2.2 | 0.05 | 99.86 |

### 3.3. Transition properties and feasibility of laser cooling CdF

The TDMs of $2^2\Pi$–$X^2\Sigma^+$ and $2^2\Sigma^+$–$X^2\Sigma^+$ were calculated as a function of the internuclear distance $R = 1.3$ Å–6.0 Å, which can be seen from Fig. 9. In the Franck–Condon region (1.6 Å–2.8 Å), the TDM of the $2^2\Pi$–$X^2\Sigma^+$ has a largest value and then gradually decreases to zero as internuclear distance longer than 4.0 Å. The TDM of the $2^2\Sigma^+$–$X^2\Sigma^+$ transition has a maximum value at $R = 2.7$ Å and decreases to zero at internuclear distance longer than 5.0 Å. The TDMs of $2^2\Pi$ and $2^2\Sigma^+$ tend to be zero due to the spin-forbidden transitions $^3P_u$–$^1S_g$ for Cd atom. The Einstein coefficients $A_{v'v''}$, Franck–Condon factors (*FCFs*), and transition energies $T_{v'v''}$ of $2^2\Pi$–$X^2\Sigma^+$ and $2^2\Sigma^+$–$X^2\Sigma^+$ transitions were evaluated and listed in Tables 5 and 6. The Einstein coefficients of $2^2\Pi$–$X^2\Sigma^+$ transition indicate that the $\Delta v(v' - v'') = 0$ bands are predicted to be more intense than the other bands due to similar equilibrium internuclear distances of the $2^2\Pi$ and $X^2\Sigma^+$ states. For the $2^2\Sigma^+$–$X^2\Sigma^+$ transition, the $(2, 23)$ band is predicted to be the most intense, which is caused by the large equilibrium distance of $2^2\Sigma^+$ state relative to that of the $X^2\Sigma^+$ state.

The radiative lifetime of vibrational level $v'$ for a given state is defined by the inverse of the total Einstein coefficient $A_{v'} = \left(\sum_{v''} A_{v'v''}\right)$. Based on the Einstein coefficients $A_{v'v''}$ given in Tables 5 and 6, the radiative lifetimes of the $2^2\Pi v' = 0$–3 and $2^2\Sigma^+ v' = 0$–3 vibrational levels to ground state were determined. The radiative lifetimes of these two sets of transitions are in the order of ten nanoseconds and hundred nanoseconds, respectively, which can be found in Table 7. In addition, the calculated spontaneous radiative lifetime of $2^2\Sigma^+$–$X^2\Sigma^+$ of isovalent molecule ZnF in recent theoretical work[36] is 10.98 ns, which is one order smaller than our calculated value (141.89 ns) of those of CdF; their calculated spontaneous radiative lifetime of $2^2\Pi$–$X^2\Sigma^+$ of ZnF is 8.21 ns, which is only 2.57 ns smaller than our evaluated value (10.78 ns) of corresponding transition of CdF. The relatively small deviation between spontaneous radiative lifetimes of low-lying states of CdF and ZnF indicates that the studies of transition properties of CdF in our work are reliable.

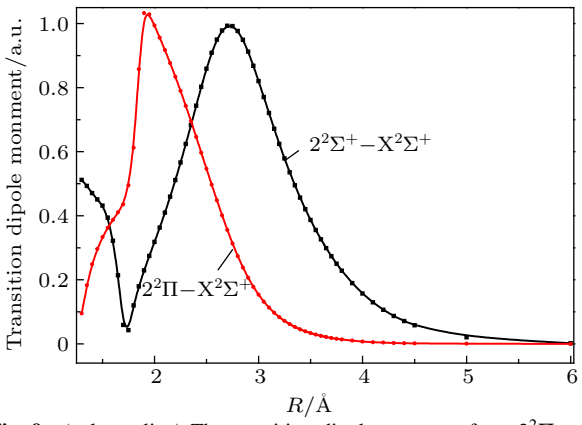



**Fig. 9.** (color online) The transition dipole moments from $2^2\Pi$ and $2^2\Sigma^+$ to $X^2\Sigma^+$.

**Table 5.** Einstein coefficients $A_{v'v''}$ ($\times 10^6$ s$^{-1}$), Franck–Condon factors (*FCFs*), and transition energies $T_{v'v''}$ (cm$^{-1}$) for the $2^2\Pi$–$X^2\Sigma^+$ transition of CdF molecule.

| $v''$ | | $v' = 0$ | $v' = 1$ | $v' = 2$ | $v' = 3$ |
|---|---|---|---|---|---|
| 0 | $A_{v'v''}$ | 89.967 | 1.5931 | 0.6244 | 0.3340 |
| | *FCFs* | 0.9691 | 0.0168 | 0.0064 | 0.0034 |
| | $T_{v'v''}$ | 35786 | 36419 | 37047 | 37659 |
| 1 | $A_{v'v''}$ | 2.3458 | 77.834 | 5.1917 | 2.1515 |
| | *FCFs* | 0.0265 | 0.8609 | 0.0558 | 0.0287 |
| | $T_{v'v''}$ | 35242 | 35875 | 36503 | 37115 |
| 2 | $A_{v'v''}$ | 0.3362 | 9.9014 | 58.508 | 8.9944 |
| | *FCFs* | 0.0039 | 0.0146 | 0.6581 | 0.0991 |
| | $T_{v'v''}$ | 34703 | 35336 | 35964 | 36576 |
| 3 | $A_{v'v''}$ | 0.0320 | 0.5668 | 23.424 | 34.769 |
| | *FCFs* | 0.0004 | 0.0068 | 0.2755 | 0.4036 |
| | $T_{v'v''}$ | 34169 | 34802 | 35430 | 36042 |

**Table 6.** Einstein coefficients $A_{v'v''}$ ($\times 10^6$ s$^{-1}$), Franck–Condon factors (*FCFs*), and transition energies $T_{v'v''}$ (cm$^{-1}$) for the $2^2\Sigma^+$–$X^2\Sigma^+$ transition of CdF molecule.

| $v''$ | | $v'=0$ | $v'=1$ | $v'=2$ | $v'=3$ |
|---|---|---|---|---|---|
| 21 | $A_{v'v''}$ | 0.9060 | 45.352 | 4.7615 | 48.022 |
| | *FCFs* | 0.1443 | 0.0553 | 0.0055 | 0.0545 |
| | $T_{v'v''}$ | 16449 | 16763 | 17076 | 17388 |
| 22 | $A_{v'v''}$ | 1.037 | 12.998 | 30.701 | 31.549 |
| | *FCFs* | 0.1416 | 0.0171 | 0.03884 | 0.0386 |
| | $T_{v'v''}$ | 16207 | 16342 | 16655 | 16967 |
| 23 | $A_{v'v''}$ | 1.0421 | 0.0378 | 49.870 | 3.7659 |
| | *FCFs* | 0.1538 | 0.0005 | 0.0680 | 0.0049 |
| | $T_{v'v''}$ | 15613 | 15928 | 16241 | 16553 |
| 24 | $A_{v'v''}$ | 0.9056 | 15.746 | 37.502 | 6.5335 |
| | *FCFs* | 0.1447 | 0.0242 | 0.0552 | 0.0092 |
| | $T_{v'v''}$ | 15208 | 15522 | 15835 | 16147 |
| 25 | $A_{v'v''}$ | 1.0378 | 48.145 | 8.4249 | 33.033 |
| | *FCFs* | 0.1580 | 0.0800 | 0.0134 | 0.0504 |
| | $T_{v'v''}$ | 14810 | 15124 | 15437 | 15749 |

**Table 7.** Radiative lifetimes of the transitions from $2^2\Pi$, $2^2\Sigma^+$ to the ground $X^2\Sigma^+$ state.

| Transition | Radiative lifetimes/ns | | | |
|---|---|---|---|---|
| | $v'=0$ | $v'=1$ | $v'=2$ | $v'=3$ |
| $2^2\Pi$–$X^2\Sigma^+$ | 10.78 | 11.11 | 11.35 | 11.77 |
| $2^2\Sigma^+$–$X^2\Sigma^+$ | 141.89 | 134.36 | 127.09 | 121.26 |

As shown in Table 5, the *FCFs* for $\Delta v(v'-v'')=0$ transitions (diagonal) of $2^2\Pi$–$X^2\Sigma^+$ have the largest factors, whereas the others (off-diagonal) have very small values, which is an important criterion for laser cooling candidate molecule. Figure 10 shows the proposed laser cooling scheme for CdF molecule. The calculated *FCFs* for 0–0 transition is $f_{00}=0.969$, which is slightly smaller than that in SrF ($f_{00}=0.98$)[5] and large enough for laser cooling. With the present scheme of CdF molecule, only one main pump laser and two repump lasers are needed. The main laser drives the main cooling transition $X^2\Sigma^+(v''=0)\rightarrow 2^2\Pi(v'=0)$ at $\lambda_{00}=279.4$ nm. The probability of decay for $2^2\Pi(v'=0)$ to $X^2\Sigma^+(v''=1)$ is small (0.027) and to $X^2\Sigma^+(v''=2)$ is even smaller (0.004). The total probability of the decays for $2^2\Pi$ ($v'=0$) to $X^2\Sigma^+$ ($v''\geq 3$) is less than $10^{-3}$. Two repump lasers with $\lambda_{10}=283.8$ nm and $\lambda_{21}=283.0$ nm are needed to excite the molecules falling from $v'=0$ to $v''=1$ ($f_{01}=0.027$) and from $v'=1$ to $v''=2$ ($f_{12}=0.015$), respectively. The lifetime of $2^2\Pi$ state is $\sim 11$ ns, which is about half of SrF,[5] ensuring the efficient laser cooling of CdF molecule. The repulsive state $1^2\Pi$ just lies below $2^2\Pi$ and the bound state $2^2\Sigma^+$ crosses with $2^2\Pi$ state, which would lead to dissociative or hot CdF molecule, therefore the efficiency of the laser cooling would be reduced.

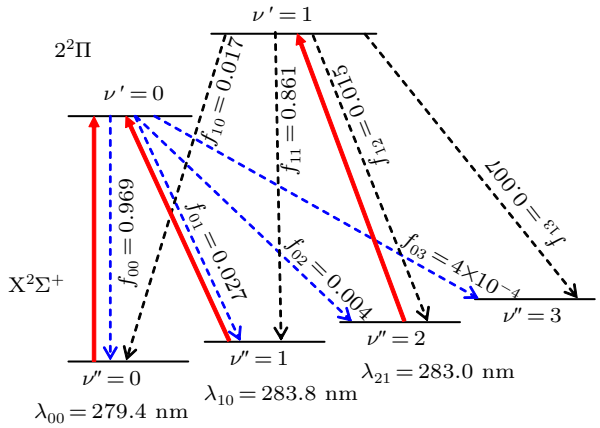



**Fig. 10.** (color online) Proposed scheme for laser cooling of CdF using the $X^2\Sigma^+\rightarrow 2^2\Pi$ transition (solid line) and decay pathways (dotted line) with $f_{v'v''}$ as shown. Here $\lambda_{v'v''}$ is the wavelength of the $X^2\Sigma^+(v'')\rightarrow 2^2\Pi(v')$ transition.

## 4. Conclusions

The PECs of 14 Λ–S electronic states of CdF correlating to the two lowest dissociation asymptotes and the DMs of $^2\Sigma^+$ and $^2\Pi$ were computed at icMRCI level. The calculated PECs show that nine electronic states ($X^2\Sigma^+$, $2^2\Sigma^+$, $2^2\Pi$, $3^2\Sigma^+$, $1^2\Delta$, $1^2\Sigma^-$, $1^4\Sigma^+$, $1^4\Delta$, $1^4\Sigma^-$) are bound and the other five electronic states ($1^2\Pi$, $3^2\Pi$, $1^4\Pi$, $2^4\Pi$, $2^4\Sigma^+$) are repulsive. Based on the computed PECs, the spectroscopic parameters of these bound Λ–S and Ω states were evaluated. The transition properties of $2^2\Pi$–$X^2\Sigma^+$ and $2^2\Sigma^+$–$X^2\Sigma^+$, including the TDMs, Einstein coefficients, *FCFs*, and radiative lifetimes, were discussed. Moreover, the feasibility and challenges for laser cooling of CdF molecule were discussed and presented. The sudden changes of the DMs and the SO matrix elements indicate the sharp changes of the electronic configurations in the avoided crossing region. Taking into account the SOC effect, there are 30 Ω states generated from the 14 Λ–S electronic states. Among these Ω states, the $(3)1/2$ and $(4)1/2$ states exchange their dominant Λ–S compositions with each other around avoided crossing region. The present theoretical results reveal more information on the electronic structures and spectroscopic properties of the low-lying states of CdF molecule.

## References


[1] Olajire A A, Ayodele E T, Oyedirdan G O and Oluyemi E A 2003 *Environ. Monit. Assess.* **85** 135
[2] Greene D P and Eden J G 1985 *Opt. Commun.* **53** 263
[3] Cuajungco M P and Fagét K Y 2003 *Brain Res. Rev.* **41** 44
[4] Tenenbaum E D, Flory M A, Pulliam R L and Ziurys L M 2007 *J. Mol. Spectrosc.* **244** 153
[5] Shuman E S, Barry J F and DeMille D 2010 *Nature* **467** 820
[6] Givan A and Loewenschuss A 1982 *J. Mol. Struct.* **78** 299
[7] Hildenbrand D L, Lau K H and Roos J W 1999 *J. Chem. Phys.* **111** 1337
[8] Elmoussaoui S, El-Kork N and Korek M 2016 *Comput. Theor. Chem.* **1090** 94
[9] Rochester G D and Olsson E 1939 *Z. Physik* **114** 495
[10] Moravec V D, Klopcic S A, Chatterjee B and Jarrold C C 2001 *Chem. Phys. Lett.* **341** 313
[11] Flory M A, McLamarrah S K and Ziurys L M 2006 *J. Chem. Phys.* **125** 194304
[12] Asundi R K, Samuel R and Zaki-Uddin M 1935 *Proc. Phys. Soc.* **47** 235
[13] Fowler C A 1942 *Phys. Rev.* **62** 141
[14] Huber K P and Herzberg G 1979 *Constants of Diatomic Molecules, Molecular Spectra and Molecular Structure*, Vol. IV (New York: Van Nostrand Reinhold)

[15] Bowmaker G A and Schwerdtfeger P 1990 *J. Mol. Struct.: THEOCHEM* **205** 295
[16] Harrison J F, Field R W and Jarrold C C 2002 *Low-Lying Potential Energy Surfaces*, Vol. 828 (Washington, DC: American Chemical Society)
[17] Hayashi S, Léonard C and Chambaud G 2008 *J. Chem. Phys.* **129** 44313
[18] Kaupp M and von Schnering H G 1994 *Inorg. Chem.* **33** 4179
[19] Liao M, Zhang Q and Schwarz W H E 1995 *Inorg. Chem.* **34** 5597
[20] Fan Q C, Sun W G, Li H D and Feng H 2012 *Chin. Phys. B* **21** 023301
[21] Zhang L L, Gao S B, Meng Q T and Song Y Z 2015 *Chin. Phys. B* **24** 013101
[22] Liu Y F, Zhai H S and Liu Y L 2015 *Eur. Phys. J. D* **69** 1
[23] Luo W, Li R, Gai Z Q, Ai R B, Zhang H M, Zhang X M and Yan B 2016 *Chin. Phys. B* **25** 073101
[24] Minaev B F, Minaeva V A and Evtuhov Y V 2009 *Int. J. Quantum Chem.* **109** 500
[25] Minaev B, Yaschuk L and Kukueva V 2005 *Acta A. Mol. Biomol. Spectrosc.* **61** 1105
[26] Werner H J, Knowles P J, Lindh R, Manby F R, Schütz M and others, MOLPRO, version 2010, a package of *ab initio* programs; see http://www.molpro.net
[27] LeRoy R J 2007 LEVEL8.0: "A computer program for solving the radial Schrödinger equation for bound and quasibound levels," University of Waterloo Chemical Physics Research Report CP-663 (2007)
[28] Peterson K A and Puzzarini C 2005 *Theor. Chem. Acc.* **114** 283
[29] Dunning T H D Jr 1989 *J. Chem. Phys.* **90** 1007
[30] Werner H J and Knowles P J 1985 *J. Chem. Phys.* **82** 5053
[31] Werner H J and Knowles P J 1988 *J. Chem. Phys.* **89** 5803
[32] Knowles P J and Werner H J 1988 *Chem. Phys. Lett.* **145** 514
[33] Berning A, Schweizer M, Werner H J, Knowles P J and Palmieri P 2000 *Mol. Phys.* **98** 1823
[34] Moore C E 1971 *Atomic Energy Levels* (Washington, DC: National Bureau of Standard)
[35] Bernath P F and McLeod S 2001 *J. Mol. Spectrosc.* **207** 287
[36] Elmoussaoui S, El-Kork N and Korek M 2017 *Can. J. Chem.* **95** 22